iScience

CellPress
OPEN ACCESS

Article

Dissecting VEGF-induced acute versus chronic vascular hyperpermeability: Essential roles of dimethylarginine dimethylaminohydrolase-1

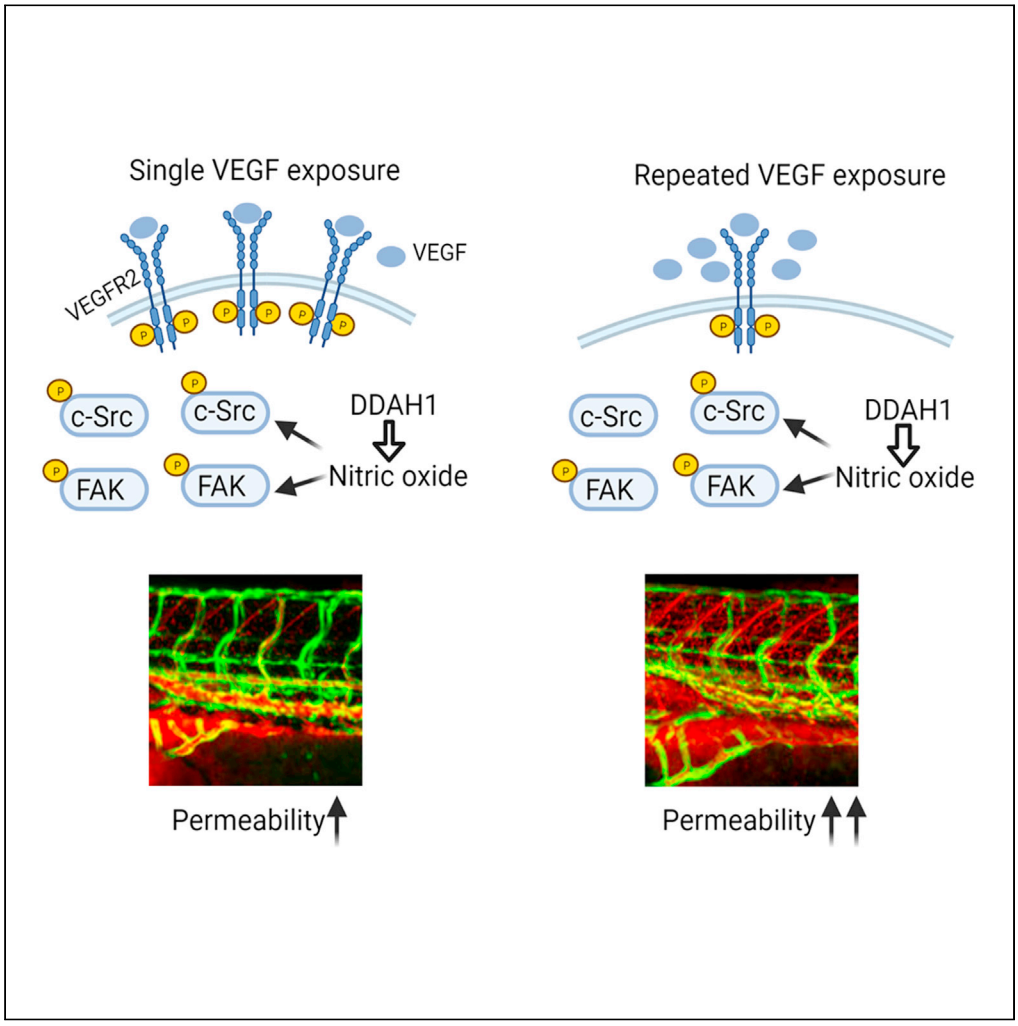

Ying Wang, Ramcharan Singh Angom, Tanmay A. Kulkarni, ..., Yingjie Chen, Roman N. Rodionov, Debabrata Mukhopadhyay

mukhopadhyay.debabrata@mayo.edu

Highlights

Chronic VEGF exposure induces a different signaling pattern in endothelial cells

A novel algorithm can precisely quantify the vascular permeability in zebrafish model

DDAH1 acts as a novel mediator of VEGF-induced vascular hyperpermeability

Wang et al., iScience 24, 103189
October 22, 2021
https://doi.org/10.1016/j.isci.2021.103189

iScience

CellPress
OPEN ACCESS

Article

Dissecting VEGF-induced acute versus chronic vascular hyperpermeability: Essential roles of dimethylarginine dimethylaminohydrolase-1

Ying Wang,[1,8,9] Ramcharan Singh Angom,[1,9] Tanmay A. Kulkarni,[1] Luke H. Hoeppner,[2,6] Krishnendu Pal,[1] Enfeng Wang,[1] Alexander Tam,[1,7] Rachael A. Valiunas,[1] Shamit K. Dutta,[1] Baoan Ji,[3] Natalia Jarzebska,[4] Yingjie Chen,[5] Roman N. Rodionov,[4] and Debabrata Mukhopadhyay[1,10,*]

SUMMARY

Vascular endothelial cell growth factor (VEGF) is a key regulator of vascular permeability. Herein we aim to understand how acute and chronic exposures of VEGF induce different levels of vascular permeability. We demonstrate that chronic VEGF exposure leads to decreased phosphorylation of VEGFR2 and c-Src as well as steady increases of nitric oxide (NO) as compared to that of acute exposure. Utilizing heat-inducible VEGF transgenic zebrafish (*Danio rerio*) and establishing an algorithm incorporating segmentation techniques for quantification, we monitored acute and chronic VEGF-induced vascular hyperpermeability in real time. Importantly, dimethylarginine dimethylaminohydrolase-1 (DDAH1), an enzyme essential for NO generation, was shown to play essential roles in both acute and chronic vascular permeability in cultured human cells, zebrafish model, and Miles assay. Taken together, our data reveal acute and chronic VEGF exposures induce divergent signaling pathways and identify DDAH1 as a critical player and potentially a therapeutic target of vascular hyperpermeability-mediated pathogenesis.

INTRODUCTION

Vascular integrity refers to the capability of the capillary wall to impede the movement of fluid or solutes driven by a physical force; it not only maintains the exchange of nutrients and water between tissues and blood in physiology, but also contributes to increased edema and inflammation in several pathological conditions, including infection with the new coronavirus (severe acute respiratory syndrome coronavirus 2, or SARS-CoV-2) which causes coronavirus disease 2019 (COVID-19) (Bates, 2010; Claesson-Welsh, 2015; Teuwen et al., 2020). Originally discovered as vascular permeability factor (VPF), vascular endothelial growth factor (VEGF) is induced by hypoxia and acts as one of the key mediators of vascular permeability through activation of VEGF receptor 2 (VEGFR2) and its downstream signaling components (Claesson-Welsh, 2015; Ferrara, 2005; Senger et al., 1983). It is widely accepted that VEGF-induced vascular permeability is increased in both acute and chronic disease conditions, such as inflammation, cancer, and wound healing. While acute vascular permeability is usually induced by a rapid exposure of vascular inducing factors, such as VEGF, chronic vascular permeability is usually used to describe the hyperpermeability of pathological angiogenesis which has disintegrated vascular barrier and enhanced permeability in chronic diseases (Curry and Adamson, 2010; Nagy et al., 2008). Notably, persistent stimulation of vascular inducing factors can induce remodeling of microvasculatures and contribute to chronic vascular permeability (Claesson-Welsh et al., 2021; McDonald, 2001), suggesting the importance of sustained stimulation of vascular inducing factors. Although many key molecules have been identified in cultured cells and murine models upon acute VEGF administration, a model in which VEGF can be chronically induced to precisely measure vascular permeability is still needed.

Previously, we have taken the advantage of optical transparency of zebrafish (*Danio rerio*) embryos and developed a transgenic heat-inducible VEGF transgenic zebrafish model in which VEGF expression can be induced by exposure to heat shock (Hoeppner et al., 2012, 2015; Wang et al., 2021). In this zebrafish model, real-time vascular leakiness can be visualized using microangiography of fluorophore-conjugated

[1]Department of Biochemistry and Molecular Biology, Mayo Clinic College of Medicine and Science, 4500 San Pablo Road South, Jacksonville, FL 32224, USA

[2]Department of Biochemistry and Molecular Biology, College of Medicine and Science, Mayo Clinic, Rochester, MN 55905, USA

[3]Department of Cancer Biology, College of Medicine and Science, Mayo Clinic, Jacksonville, FL 32224, USA

[4]Department of Internal Medicine III, Technische Universität Dresden, 01307 Dresden, Germany

[5]Department of Physiology & Biophysics, University of Mississippi Medical Center, Jackson, MS 39216, USA

[6]Present address: The Hormel Institute, University of Minnesota, Austin, MN 55912, USA

[7]Present address: Sidney Kimmel Medical College, Thomas Jefferson University, Philadelphia, PA 19107, USA

[8]Present address: Department of Cardiovascular Medicine, College of Medicine and Science, Mayo Clinic, Rochester, MN 55905, USA

[9]These authors contributed equally

[10]Lead contact

*Correspondence: mukhopadhyay.debabrata@mayo.edu

https://doi.org/10.1016/j.isci.2021.103189

dextran. One challenge of data quantification in the conventional vascular permeability models is how to distinguish the extravasated dye from the dye which bound to the surface layer of the endothelium or in circulation. In the present study, we developed an algorithm to precisely quantify the vascular permeability induced by acute and chronic exposure of VEGF in the zebrafish models. We demonstrate that VEGF induces vascular permeability in a spatial-dependent manner and that acute and chronic VEGF exposures stimulate distinct levels of vascular permeability in the zebrafish models.

VEGF induces vascular hyperpermeability by binding to its cognate receptors, preferentially VEGFR2, and activating downstream signaling components (Shibuya, 2011). Tyrosine phosphorylation of VEGFR2, especially at tyrosine 951, and several intracellular signal transducers, including focal adhesion kinase (FAK) and proto-oncogene c-Src, have been shown to play critical roles in vascular permeability (Dvorak, 2021; Sun et al., 2012; Weis et al., 2004). Studies using *in vivo* models of chronic vascular permeability, including tumor models, have reported that calcium influx, c-Src, caveolin, SH2 domain-containing protein 2A (SH2D2A, VRAP, TSAD), and nitric oxide, are involved in chronic VEGF-induced vascular permeability (Bates et al., 2001; Criscuoli et al., 2005; Fukumura et al., 2001; Gratton et al., 2003; Lin et al., 2007); however, the differences between acute and chronic VEGF-induced signaling pathways, including levels of VEGFR2 and its downstream signaling mediators, were not compared. In this study, we demonstrate that chronic VEGF exposure induces different patterns of VEGFR2-FAK-c-Src signaling cascade as compared to that of acute exposure, in endothelial cells (ECs). Chronic VEGF exposure also induces a persistent increase of nitric oxide (NO) levels.

Dimethylarginine dimethylaminohydrolase-1 (DDAH1) maintains vascular homeostasis by degrading asymmetric dimethylarginine and L-N^G-monomethylarginine, two known endogenous inhibitors of endothelial NO synthase (eNOS) (Cooke and Ghebremariam, 2011). Previous studies have reported that DDAH1 promotes angiogenesis *in vitro* and *in vivo* (Achan et al., 2005; Dowsett et al., 2015; Zhang et al., 2013), but its role in VEGF-induced vascular hyperpermeability remains unclear. Here, we show that protein-translation blocking morpholino (MO)-mediated knockdown of DDAH1 decreases both VEGF-mediated acute and chronic vascular hyperpermeability. The effect of DDAH1 on vascular permeability was further validated in DDAH1 knockout mice and transgenic mice overexpressing DDAH1 using peripheral permeability assays. Taken together, we utilize a novel algorithm to analyze the vascular permeability in an established heat-inducible VEGF transgenic zebrafish model, which reveals different levels of vascular permeability upon acute and chronic VEGF stimulation. Our results suggest the DDAH1-NO pathway plays an essential role in VEGF-induced acute and chronic vascular permeability.

RESULTS

Acute and chronic VEGF exposures induce distinct patterns of signaling cascade activation

To dissect the molecular mechanism of VEGF-induced acute and chronic vascular permeability, we examined the phosphorylation of VEGFR2 and its downstream signal transducers including FAK and c-Src, a signaling cascade shown to be required for VEGF-induced vascular permeability previously (Sun et al., 2012; Weis et al., 2004). Acute and chronic VEGF exposures were induced in HUVECs by a single incubation of VEGF (10 ng/mL) and three times of VEGF stimulation separated by 30 min intervals, respectively. Consistent with previous studies (Sun et al., 2012; Weis et al., 2004), acute VEGF exposure induced phosphorylation of VEGFR2 tyrosine 1175 and 951, FAK tyrosine 397, and c-Src tyrosine 416. However, a different pattern of activation of this signaling pathway was observed upon chronic VEGF stimulation. While a similar level of FAK phosphorylation was induced in HUVECs exposed to chronic VEGF stimulation, the protein level of VEGFR2 was reduced to 47% $\pm$ 17% of control and the phosphorylation of c-Src was only slightly induced (1.1 $\pm$ 0.3 fold change, compared to control) (Figures 1A, 1B, and S1). NO is known to be an important component in VEGF-induced permeability through mediating activation of soluble guanylyl cyclase-protein kinase G pathway and S-nitrosation of adherens junction proteins (Mayhan, 1994; Ramirez et al., 1995, 1996; Wu et al., 1996; Yuan et al., 1992). Levels of NO were then quantified with DAF-FM fluorescent probes and showed that acute and chronic VEGF stimulation induced a steady increase of NO levels in HUVECs (acute VEGF: 1.6 $\pm$ 0.2 fold change, chronic VEGF: 2.4 $\pm$ 0.4 fold changes, compared to control) (Figure 1C). Furthermore, L-NAME, an antagonist of nitric oxide synthase of NOS, was administrated. Interestingly, L-NAME did not significantly alter VEGF exposure-induced c-Src activation and VEGFR2 levels but reversed phosphorylated FAK levels in HUVECs upon acute and chronic VEGF stimulation (Figure 1A). These results indicate that NO is involved in both acute and chronic VEGF-induced signaling pathways

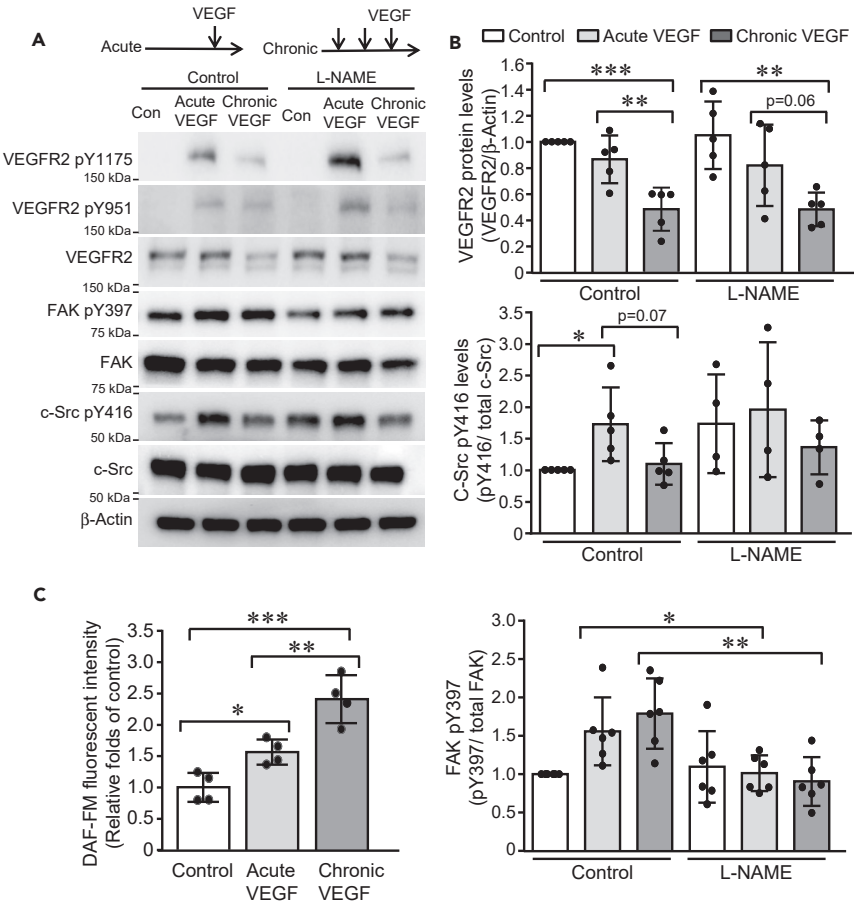

Figure 1. Acute and chronic VEGF exposures induce distinct pattern of signaling cascade activation

(A and B) HUVECs were cultured in low-serum EMB for 4 h and then exposed to single stimulus of VEGF (10 ng/mL) and three stimuli of VEGF (10 ng/mL) with 30-min intervals, respectively. Cell lysates were collected 10 min after VEGF stimulation and subjected to western blotting (A). Band intensities were analyzed and compared (N = 5 for each group) (B).

(C) HUVECs were labeled with DAF-FM (2.5 μM) and then exposed to acute and chronic VEGF stimulation, respectively. DAF-FM fluorescence was measured at Excitation/Emission of 495/515 nm and expressed as relative folds of control group. Data is representative of 3 independent experiments and expressed as mean ± SD. *, p<0.05, **, p<0.01, ***, p<0.001.

in ECs; however, chronic VEGF exposure results in decreased VEGFR2 expression and thus concomitantly reduced phosphorylation of downstream c-Src protein.

VEGF-mediated acute and chronic vascular hyperpermeability

To assess VEGF-induced acute and chronic vascular permeability, a double transgenic zebrafish system was generated by crossing the heat-inducible VEGF transgenic zebrafish (*Danio rerio*) model in which VEGF expression is driven by a heat-inducible HSP70 promoter and preceded by an upstream floxed mCherry gene (Hoeppner et al., 2012), and the *Tg (fli*:EGFP) fish (Figure 2A), in which enhanced GFP is expressed in the entire vasculature (Lawson and Weinstein, 2002). The individual F1 zebrafish line which displayed high mCherry expression upon the heat-shock induction was selected for continued work (Figure 2A). Then Cre mRNA was microinjected into single cell embryos to excise the mCherry gene, resulting in expression of hVEGF upon induction of the HSP70 promoter (Figure 2B). Microangiography was performed using Texas Red-dextran of 70 kDa as a permeabilizing tracer. Acute and chronic VEGF induction were achieved by a single incubation at 37°C for 30 min and three times of incubation at 37°C for 30 min separated by 30 min intervals at 28.5°C, respectively. The induction of VEGF was confirmed with qPCR (Figure S2). Z-stack images of zebrafish embryos were collected immediately after heat-shock (Figure 2B).

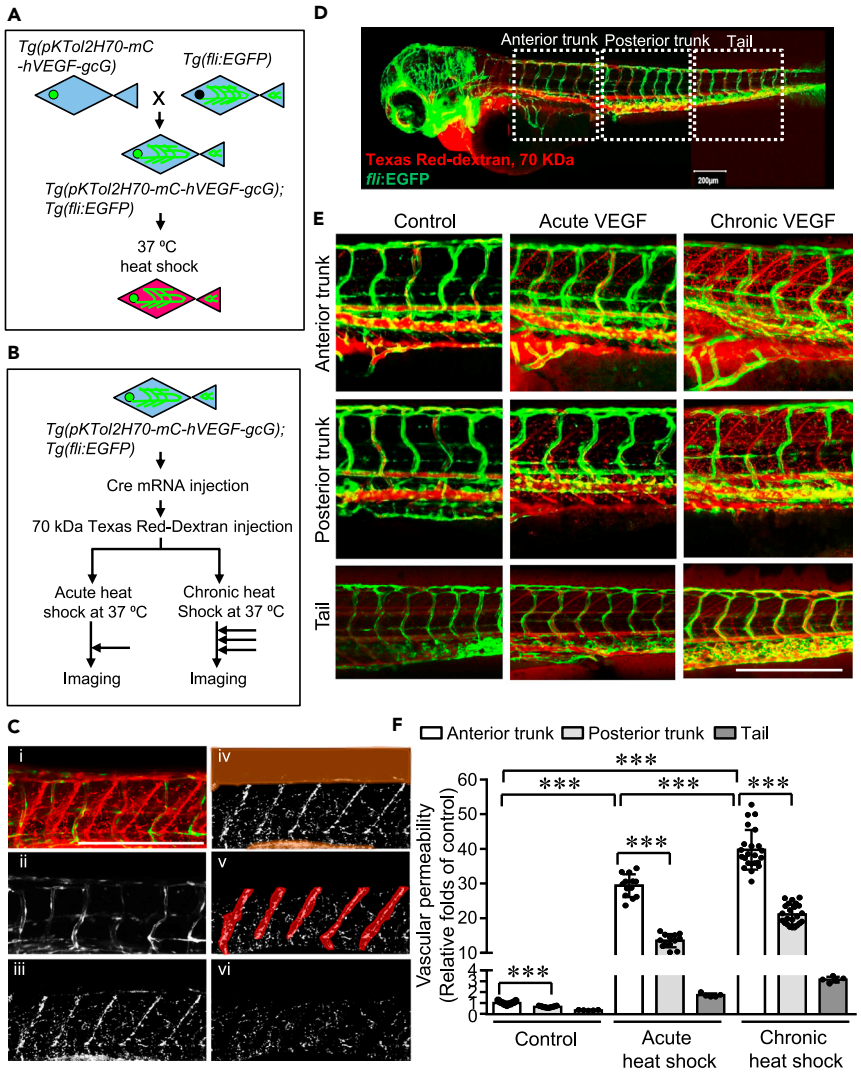

Figure 2. Quantification of the spatial distribution of vascular permeability induced by acute and chronic VEGF in zebrafish

(A) Heat-inducible VEGF transgenic zebrafish (*pKTol2H70-mC-hVEGF-gcG*) (Hoeppner et al., 2012), in which VEGF expression is driven by a heat-inducible HSP70 promoter and preceded by an upstream floxed mCherry gene, were bred with *Tg(fli:EGFP)* zebrafish (Lawson and Weinstein, 2002) to generate the double transgenic zebrafish *Tg(pKTol2H70-mC-hVEGF-gcG);Tg(fli:EGFP)*. F1 progenies were used to identify true transgenics and the lines with low background but high heat-shock induction of mCherry were selected.

(B) In the selected double transgenic zebrafish lines, Cre mRNA was microinjected into F1 single cell embryos to excise the mCherry gene, resulting in expression of hVEGF on induction of the HSP70 promoter. At 3-days postfertilization (3-dpf), zebrafish embryos were anaesthetized and microinjected with Texas Red-dextran (70 kDa) to the pericardium. VEGF-induced vascular hyperpermeability in zebrafish was examined at base line (no exposure to heat shock), upon acute (37°C for 30 min) and chronic (3 times of 37°C for 30 min with 30 min intervals at 28.5°C) exposure to heat shock as demonstrated.

(C) An image processing method was developed to analyze the vascular permeability: (1) Maximum intensity projection image was first generated, and then (2) binary mask extracted from green channel was generated. (3) Binary image constituting of red pixels was obtained after masking original image (1) by green channel (2). In addition to vascular leakiness, the resulting red pixels (Texas Red-dextran at 70 kDa) represent leakiness and signals from autofluorescence, caudal veins and arteries, and somites. (4) Pixels corresponding to autofluorescence as well as caudal arteries and veins and (5) somites were highlighted and eliminated. (6) The final processed image containing pixels show the total leakiness.

Figure 2. *Continued*
(D and E) Images of whole mount imaging (D) and different regions of zebrafish (E) were acquired immediately after heat-shock using a Zeiss LSM 880 confocal microscope using standard FITC and dsRed filter sets.
(F) Using our new algorithm, the vascular permeability of anterior and posterior regions of trunks and tail regions were analyzed and compared. ***, $p<0.001$. Zebrafish numbers in each group are presented in the scatter plot. Data is expressed as mean ± SD. Scale bar, 200 μm in (C, D, and E)

To precisely quantify the vascular hyperpermeability in the zebrafish model, we scripted a Matlab code incorporating robust thresholding and segmentation technique to precisely quantify vascular leakiness. A representative colored image file corresponding to the mid-region of the zebrafish imported in Matlab represents maximum intensity projection image (Figure 2C-i), which constitutes all the z-stacks overlapped to form a 2D image preserving maximum information. Using thresholding algorithm, we generated a binary mask to eliminate all the green pixels corresponding to enhanced GFP in all the vasculatures. The resulting image comprised of red pixels constituting noise due to autofluorescence, minor vessels and capillaries as well as permeability. To further segregate hyperpermeability, we used segmentation algorithm to manually eliminate autofluorescence, minor vessels, and capillaries by constructing segments. To distinguish between the leakage and capillaries, the corresponding 3D image was used to monitor the continuity in red pixels in different planes (Videos S1, S2, and S3). Red pixels representing leakage were observed to be mostly discrete spots as opposed to the capillaries which were continuous and more prominently observed from the 3D image. After elimination of the unwanted features represented by the red dye, the total leakage was determined by quantifying the remaining red pixels (Figure 2C-vi).

Furthermore, we applied this algorithm and analyzed the spatial distribution of vascular hyperpermeability of different regions: anterior trunk, posterior trunk and tail regions (Figure 2D). We observed that chronic VEGF stimulation induces greater overall vascular hyperpermeability, compared with acute VEGF stimulation (Figures 2E and 2F). Meanwhile, the vascular permeability showed gradual decreased levels from the anterior trunk to posterior trunk and tail regions, indicating that a spatial-dependent manner is involved.

Our results show that the repeated heat shock exposure results in a much greater level of VEGF mRNA (Figure S1) than the acute exposure, so a dose response and a time response are potentially involved in chronic VEGF exposure-induced vascular hyperpermeability. To tease out the impact of time response, we measured the vascular permeability at different time points, specifically immediately and 1.5 hr after a single heat shock (Figure S3), and observed mild differences in vascular permeability between the two points. Previous studies suggest that VEGF-induced vascular permeability occurs in a biphasic manner which exhibits an initial transient increase lasting just a few minutes and then is followed by a sustained increase that lasts many hours (Bates, 2010). Our results raise possibilities that the initial transient increase of vascular permeability predominantly contributes to the vascular leakiness. Given that our results showing that chronic induction of VEGF induces a more dramatic increase of vascular permeability (Figure 2), it is likely that the dose response, rather than the time response of VEGF, contributes to the increased vascular permeability after chronic VEGF exposure.

Knockdown of DDAH1 reduces both acute and chronic VEGF-mediated phosphorylation of FAK and c-Src in ECs

One clear difference between acute versus chronic exposure of VEGF to ECs is NO generation (Figure 1C), despite the observation that VEGFR2 expression and corresponding c-Src activation are reduced. As DDAH1 is the key modulator of NO production (Achan et al., 2005; Dowsett et al., 2015; Zhang et al., 2013), we investigated the role of DDAH1 in acute and chronic VEGF exposure-induced NO generation and downstream signaling pathways. Acute and chronic stimulation of VEGF mildly, but not significantly, affect the expression of DDAH1 in ECs (Figures 3A, S4, and S5E). Furthermore, our results show that knockdown of DDAH1 did not significantly affect the levels of either total VEGFR2 or its phosphorylation status, including phosphorylation at Y1175 and Y951. However, DDAH1 ablation did reduce the phosphorylation of both FAK and c-Src (Figures 3A, S4, and S5E), which was accompanied by decreased NO levels, quantified with fluorescent probe, DAF-FM (Figure 3B), and total nitrite/nitrate levels in the conditioned medium of control and DDAH1 knockdown ECs (Figure S5F). Conversely, overexpression of DDAH1 did not significantly change the phosphorylation of VEGFR2 but enhanced the activation of c-Src at both basal levels as well as upon VEGF acute and chronic stimulation (Figures 3C, S6, and S7). The inductive effect of DDAH1 on phosphorylation of c-Src was reversed by L-NAME, indicating that overexpression of DDAH1 enhances

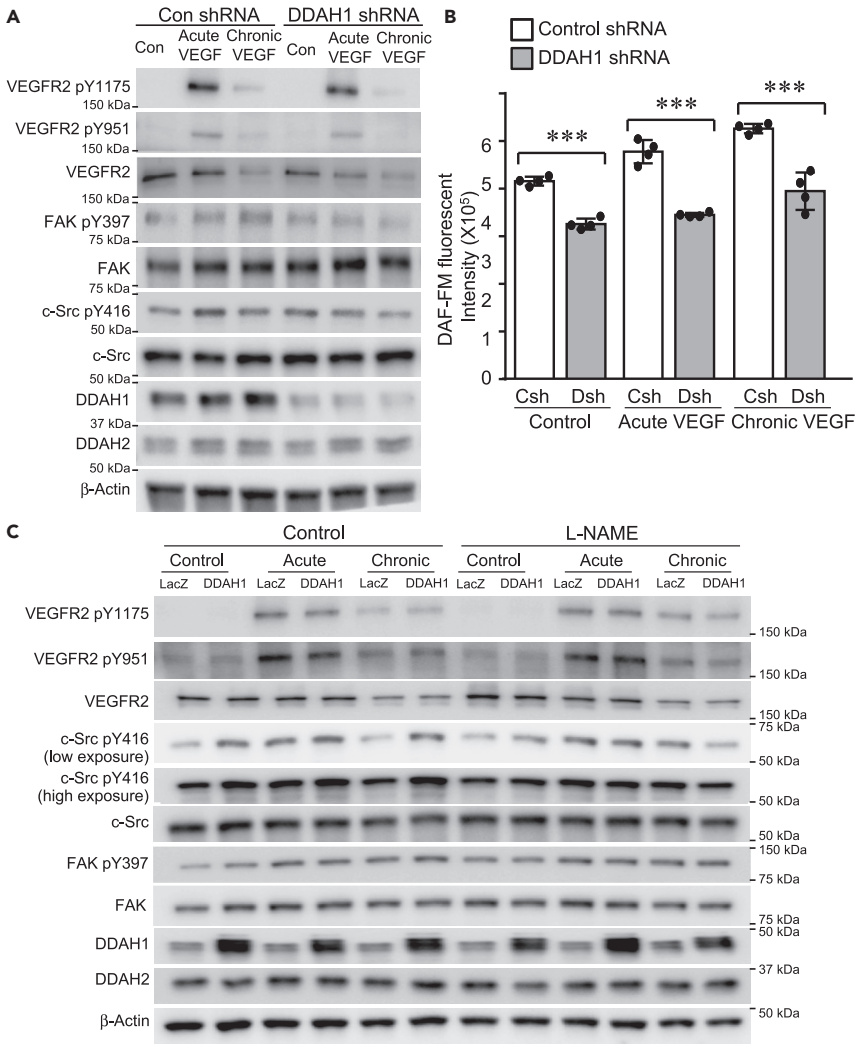

Figure 3. DDAH1 mediates acute and chronic VEGF-mediated signaling pathways in ECs

(A) HUVECs were infected with lentivirus expressing of control shRNA and DDAH1 shRNA, cultured in low-serum EMB for 4 h and then exposed to stimuli of acute (single stimulus of VEGF at 10 ng/mL) and chronic VEGF (three stimuli of VEGF at 10 ng/mL with 30 min intervals), respectively. Proteins were collected 10 min after VEGF stimulation and analyzed with western blotting (A).

(B) Control and DDAH1 knockdown HUVECs were labeled with DAF-FM (2.5 μM) and then exposed to acute and chronic VEGF stimulation, respectively. DAF-FM fluorescence was measured at Excitation/Emission of 495/515 nm. N numbers are presented in the scatter plot. Data is expressed as mean ± SD. ***, $p < 0.001$.

(C) HUVECs were infected with retrovirus expressing of LacZ and DDAH1, cultured in low-serum EMB and then exposed to acute and chronic VEGF stimulation. Proteins were collected 10 min after VEGF stimulation and analyzed with western blotting.

c-Src activation through NO (Figures 3C and S7). These results collectively suggest that DDAH1 is required for the VEGF-induced activation of FAK and c-Src pathways as well as production of NO in ECs.

Knockdown of DDAH1 decreases VEGF-induced acute and chronic vascular hyperpermeability in zebrafish

The regulatory effect of DDAH1 on acute and chronic VEGF-induced signaling pathways prompted us to next evaluate the role of DDAH1 in VEGF-induced acute and chronic vascular permeability *in vivo*. One-cell stage double transgenic zebrafish embryos *Tg(pKTol2H70-mC-hVEGF-gcG);Tg(fli:EGFP)* were injected Cre mRNA and DDAH1 MOs. Normal development of ISVs was observed, suggesting knockdown of DDAH1 did not affect the ISV development (Figure 4A). Decreased protein levels of DDAH1 were

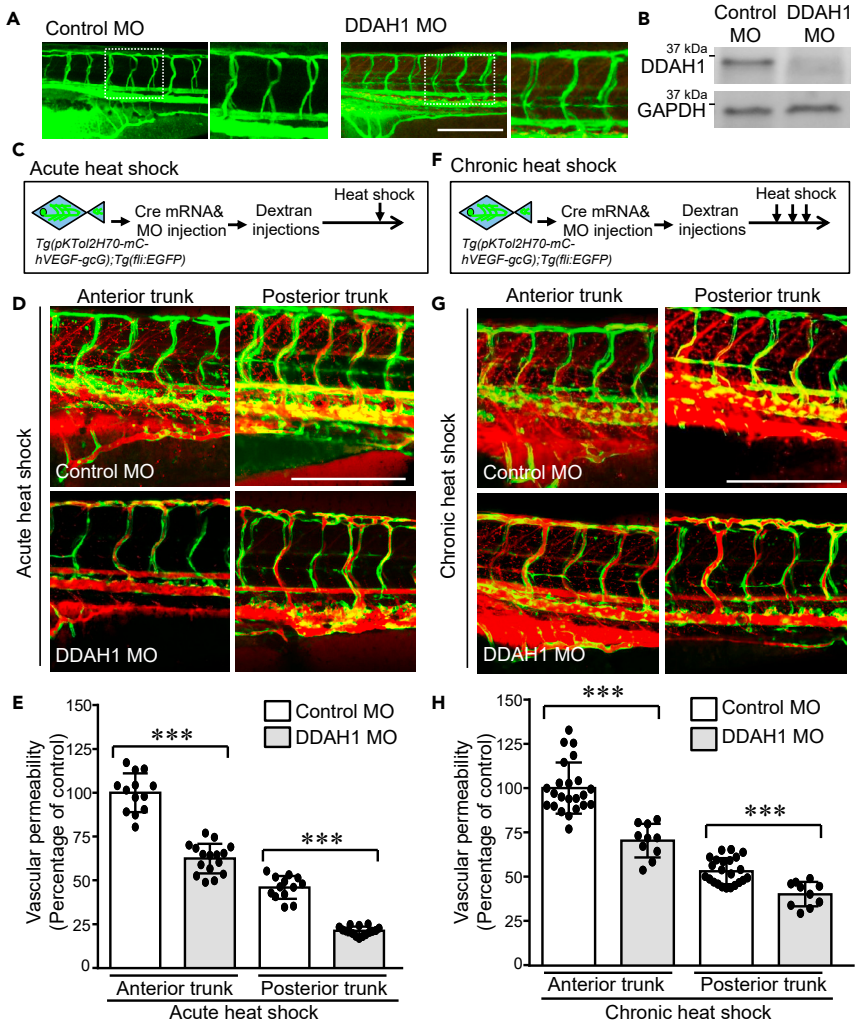

Figure 4. Knockdown of DDAH1 reduces VEGF-mediated acute and chronic vascular hyperpermeability

Double transgenic zebrafish *Tg(pKTol2H70-mC-hVEGF-gcG);Tg(fli:EGFP)* were injected with Cre mRNA and DDAH1 or control morpholino (100 μM, 4.5 nL) at one-cell stage and then microinjected Texas Red-dextran (70 kDa) to the pericardium at 3-dpf.

(A) Alignment of ISVs was analyzed.

(B) Zebrafish embryos were collected and subjected to western blotting to confirm the decrease of DDAH1 protein levels.

(C–F) Control and DDAH MO-injected zebrafish embryos were exposed to a single stimulus of heat shock at 37°C for 30 min (C and D) and three times of incubation at 37°C for 30 min separated by 30-min intervals at 28.5°C (F–G). Zebrafish embryos were imaged (D, G) and the vascular permeability of anterior and posterior trunk regions were quantified with our algorithm and compared (E and H). ***, $p < 0.001$. Zebrafish numbers in each group are presented in the scatter plot. Data is expressed as mean ± SD. Scale bar, 200 μm, in (A, D, and G).

confirmed by Western blotting (Figure 4B). After receiving the injection of Texas Red-dextran of 70 kDa as a tracer of hyperpermeability, control and DDAH1 MO-injected zebrafish embryos were subjected to acute and chronic VEGF induction. Z-stack images of zebrafish embryos were acquired, and permeability was quantified using our algorithm (Figures 4C and 4F). Our results show that upon acute VEGF exposure, decreased accumulation of Texas Red-dextran was observed in both the anterior and posterior trunk regions of DDAH1 MO-injected zebrafish embryos (Figures 4C and 4D). Quantification of vascular permeability using our algorithm confirmed that the vascular permeability was significantly decreased in DDAH1 knockdown zebrafish embryos (Figure 4E). Similarly, knockdown of DDAH1 significantly reduced the chronic VEGF-induced vascular permeability in both the anterior and posterior trunk regions of

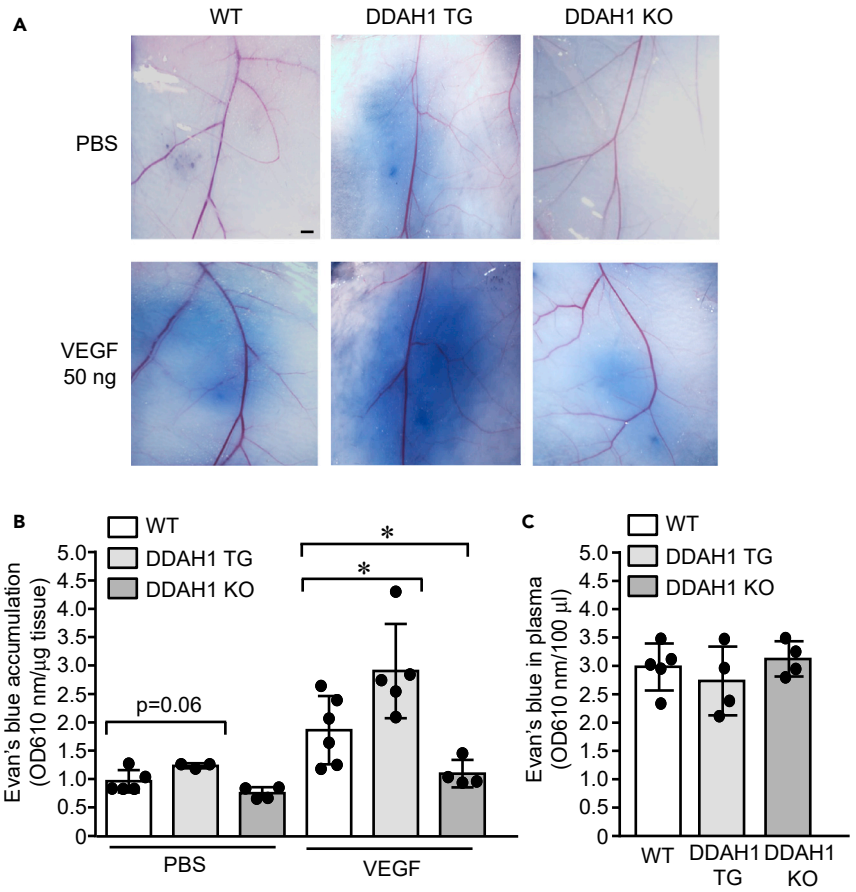

Figure 5. Vascular leakiness was enhanced in DDAH1 transgenic mice but reduced in DDAH1 knockout mice

(A–C) Sex- and age-matched wild type (WT), DDAH1 transgenic (TG) and DDAH1 knockout (KO) mice were subjected to Miles assay. Evans blue (1%) were intravenously injected according to body weight and then intradermal injection of VEGF (50 ng) and PBS was performed. Skin was dissected and imaged (A) and Evans blue was quantified after extraction with formamide and normalized to tissue weight (B). Plasma was also collected at the endpoint to show comparable level of Evans blue in the circulation (C). *, $p<0.05$. Animal numbers in each group are presented in the scatter plot. Data is expressed as mean ± SD. Scale bar, 1 mm, in (A)

zebrafish embryos (Figures 4F and 4H), supporting that DDAH1 is required for VEGF-induced both acute and chronic vascular hyperpermeability in zebrafish model.

Vascular hyperpermeability was reduced in DDAH1−/− mice and enhanced in DDAH1 transgenic mice in Miles assay

Our results in zebrafish embryos (Figure 4) and cultured HUVECs (Figure 3) strongly support the essential role of DDAH1 in VEGF-induced vascular hyperpermeability. Thus, the regulatory role of DDAH1 on vascular permeability was further validated in the mouse Miles assay. Wild-type (WT), DDAH1 transgenic mice with genomic overexpression of human DDAH1 under control of β-actin promoter (Dayoub et al., 2003), and genomic DDAH1 knockout mice (Hu et al., 2011) were administrated an intradermal injection of VEGF and local accumulation of intravenously delivered Evans blue was quantified. Our results (Figures 5A and 5B) show that PBS did not induce extravasation of Evans blue in WT or DDAH1 knockout mice but increased the Evans blue accumulation at the injection sites of DDAH1 transgenic mice, indicating increased vascular permeability. Furthermore, VEGF-induced extravasation of Evans blue was greatly enhanced in DDAH1 transgenic mice but inhibited in DDAH1 knockout mice. The blood was collected and showed comparable levels of Evans blue in the circulation (Figure 5C). Collectively, these results from DDAH1 transgenic and knockout mice support the important roles of DDAH1 in vascular permeability in mice.

DISCUSSION

VEGF is well known for its role in physiological angiogenesis during embryonic vascular development, growth, and tissue repair and for its function in the regulation of pathological angiogenesis in several disease conditions (Carmeliet et al., 1996). However, originally designated as VPF, VEGF is a potent factor of inducing vascular hyperpermeability. The effect of VEGF on vascular permeability has been studied in several models, in which a single stimulus of VEGF was administered to cultured cells or animals. However, persisted stimulation of VEGF has been recognized to induce remodeling of microvasculatures and contribute to the hyperpermeability vascular permeability in chronic diseases (Claesson-Welsh et al., 2021; McDonald, 2001). In this study, we took advantage of the heat-inducible VEGF transgenic zebrafish model to induce acute and chronic VEGF expression by exposing zebrafish to heat shock a single time and multiple times, respectively. Given the ease of MO-mediated gene knockdown and development of new genome editing technologies including clustered regularly interspaced short palindromic repeats (CRISPR), the chronic vascular permeability model in zebrafish will be valuable to understand the molecular mechanism and screen novel molecular modulators of vascular permeability.

In this study, we developed a sophisticated method to precisely induce chronic VEGF induction and quantify the vascular hyperpermeability. We performed microangiography using Texas Red-dextran of 70 kDa as a permeabilizing tracer in the double transgenic zebrafish, and developed a Matlab-coded algorithm to quantify VEGF-induced vascular leakiness. Maximum intensity projection images were generated, which are commonly used in several previous studies of vascular permeability (Chen et al., 2017; Heneweer et al., 2011; Lagendijk et al., 2017; Pink et al., 2012; Rygh et al., 2011), and then processed with the new algorithm incorporating robust thresholding and segmentation techniques. With this algorithm, we were able to remove signals of permeabilizing tracer within ISVs, small vessels, and capillaries, as well as those generated from auto-fluorescence and somite, in the analysis of vascular permeability. Use of segmentation algorithm allowed us to manually eliminate regions representing minor vessels and capillaries, which makes this algorithm robust and precise. Thus, the concept of this new algorithm is a considerable strength of this study and will also provide insights in the quantification of vascular permeability in other *in vitro* and *in vivo* models. One potential limitation of our algorithm is that some signal corresponding to the vascular leakiness may be discarded during image processing due to manual error, even though corresponding 3D images were used to confirm the vasculatures, including minor vessels and capillaries, before signaling elimination. However, we maintain consistency in eliminating pixels adjacent to the vessels that correspond to the autofluorescence signal in all the images. In the future, we would work on utilizing a more robust algorithmic approach with minimal manual intervention that would aid us in making our approach more optimal. Another potential limitation is that our algorithm cannot determine the contribution of VEGF-induced vasodilation in vascular leakiness.

One interesting result we observed is that chronic VEGF exposures strikingly reduce protein level of VEGFR2 as well as phosphorylated VEGFR2, but steadily increase NO generation in cultured ECs, which is accompanied with enhanced vascular permeability in the zebrafish model (Figure 1). The protein level of VEGFR2 is tightly controlled through multiple mechanisms including endocytosis-recycling axis (Zhang and Simons, 2014). Prolonged VEGF exposure for 30 min was shown to reduce the levels of VEGFR2 by ~40% in ECs (Gampel et al., 2006). Accordingly, in VEGF-producing squamous cell carcinoma, tumor-associated ECs exhibit reduced levels of VEGFR2, compared to normal oral mucosa endothelium (Domigan et al., 2015; Zhang et al., 2010). Our results raised the possibility that the effect of VEGF on NO generation and vascular permeability is sustained, even when the expression level of VEGFR2 and its phosphorylation is greatly reduced. It is likely that the cumulative effect of multiple VEGF exposures contributes to the enhanced NO generation and vascular permeability in the chronic VEGF stimulation. Other possible mechanism including the potential heterodimer of VEGFR2 with VEGFR1/3 (Cudmore et al., 2012; Gampel et al., 2006; Huang et al., 2001; Murakami et al., 2008; Yang et al., 2014) may be involved.

Our results show that VEGF stimulation does not significantly increase the protein levels of DDAH1 (Figure 3). However, acute and chronic VEGF exposure-induced of NO and vascular permeability are decreased in DDAH1 knockdown cells and zebrafish embryos, respectively, it is thus likely that DDAH1 constitutively contributes to VEGF-induced NO and vascular permeability. NO is required for VEGF-induced hyperpermeability through mediating activation of soluble guanylyl cyclase-protein kinase G pathway and S-nitrosation of adherens junction proteins (Mayhan, 1994; Ramirez et al., 1995, 1996; Wu et al., 1996; Yuan et al., 1992). Consistent with previous studies showing that eNOS acts as a downstream

of c-Src (Di Lorenzo et al., 2013; Duval et al., 2007), our results show that L-NAME, an inhibitor of NO synthesis, did not significantly alter levels of phosphorylated c-Src in the presence of acute and chronic VEGF exposures. In contrast, L-NAME partially reversed the phosphorylation of FAK tyrosine 397, supporting that VEGF-stimulated FAK tyrosine 397 phosphorylation occurs independently of c-Src (Liang et al., 2010). Interestingly, L-NAME was shown to inhibit the phosphorylation of both FAK and c-Src in DDAH1 overexpressing HUVECs, which have greater basal level of NO (Dayoub et al., 2003). These results suggest that the levels of NO or its bioavailability tightly controls the downstream signaling pathways. Although DDAH1 is known as an enzyme which breaks down ADMA to promote NO generation, recent literature has demonstrated a potential ADMA-independent mechanism also mediates the effect of DDAH (Hulin et al., 2019a; Yuan et al., 2014; Zhang et al., 2011). Indeed, our results show that DDAH1 knockdown causes additional inhibition of VEGF-induced activation of c-Src compared to L-NAME. The effect of DDAH1 on VEGF-induced signaling pathways was also validated in primary human retinal ECs. Our results show that knockdown of DDAH1 inhibited acute VEGF exposure-induced phosphorylation of FAK and c-Src (Figures S8 and S9). However, repeated stimulation of VEGF did not sustain the activation of FAK, indicating heterogeneous mechanism may be involved in different types of ECs.

Previous studies indicate that DDAH1 promotes angiogenesis which involves regulation of endogenous VEGF levels. Interestingly, these cells showed similar proliferative response to exogenously supplemented VEGF, compared with control cells (Zhang et al., 2013), suggesting that DDAH1 is not required for all the signaling transduction downstream of VEGF, especially those essential for cell proliferation. The quantification of total and phosphorylated levels of VEGFR2 in DDAH1 knockdown levels (blots shown in Figure 3A) further confirmed that DDAH1 knockdown slightly decreased the protein levels of VEGFR2 but did not significantly affect its phosphorylation induced by single and multiple exposure of VEGF (Figure S5). Notably, the systolic blood pressure of DDAH1 transgenic mice were reported previously to be ~13 mm Hg lower than that of control mice (Dayoub et al., 2003), while the global DDAH1 knockout mouse line used in this study exhibited ~20 mm Hg increase in mean aortic blood pressure (Hu et al., 2011). Since blood pressure can potentially affect the blood flow in microvasculature and can indirectly contribute to vascular hyperpermeability (Claesson-Welsh, 2015), our current data cannot exclude the possibility that DDAH1-mediated blood pressure regulation indirectly controls vascular permeability.

One prime example of vascular permeability induced by chronic VEGF expression may be hemangioma of infancy, which is a noncancerous vascular tumor with elevated VEGF expression and leaky vessels (Lin and Schwartz, 2006; Seamens et al., 2018). It is likely that DDAH1 is potentially involved in the vascular leakiness of hemangioma of infancy and regulated by propranolol, which effectively treats large and morbid hemangiomas of infancy through a molecular mechanism independent of its beta blockade activities (Sasaki et al., 2019).

DDAH1 is known to mediate the establishment of vascular network in several types of cancers and DDAH1 inhibitors have been reported to reduce the tumor growth in rodent cancer models (Buijs et al., 2017; Hulin et al., 2019a, 2019b; Kostourou et al., 2002, 2003). Our study suggests that DDAH1-mediated hyperpermeability is potentially involved in cancer pathogenesis. Additionally, increased vascular hyperpermeability is an important pathological step in several other disease conditions, including COVID-19-related pulmonary edema (Teuwen et al., 2020). Our results emphasized the critical role of DDAH-NO pathway and indicate that targeted-inhibition of DDAH-NO pathway will be potential therapeutic targets in the treatment of these diseases.

Limitations of the study

The single and multiple doses of VEGF stimulation in our experiment design certainly cannot recapitulate all the aspects of acute and chronic vascular permeabilities; however, given the important roles of sustained stimulation of VEGF in chronic vascular permeability, we anticipate our study will help to understand the signaling patterns induced by single and multiple stimulations of VEGF, which provide insights to understand the molecular mechanism of acute and chronic vascular permeability.

In this study, we injected Evans blue dye in the mouse models to measure vascular permeability. Since its initial application by Dr. Herbert McLean, Evans blue and its derivatives have been widely used in the studies of vascular permeability and theranostic studies due to their high water solubility, slow excretion and tight binding to serum albumin (Cooksey, 2014; Evans and Schulemann, 1914). Notably, Evans blue

has shown to be pharmacologically active and acts as inhibitors of AMPA/kainate receptor, L-glutamate uptake and sodium channel subunit at nanomolar levels (Price and Raymond, 1996; Schurmann et al., 1997; Yamamura et al., 2005). In our experiments, 100 μL of 1% Evans blue was intravenously administrated to mice weighing 30 grams. Given that the blood volume of mice is approximately 77–80 μL/g, the circulating concentration of Evans Blue is 433–450 μM. Although previous kinetic studies show that more than 99% of Evans blue becomes fully albumin-bound in blood (Freedman and Johnson, 1969; Yao et al., 2018), it is still likely that both free and albumin-bound Evans blue potentially inhibits neurotransmitter signaling and indirectly affects vascular permeability.

Zebrafish has been widely accepted in the studies of development and diseases due to several advantages including conservation of the molecular pathways between fish and mammals (Chavez et al., 2016). However, discrepancies in signaling pathways between zebrafish and mammals are still present (Ung et al., 2010). One of the major differences is that zebrafish has four VEGF receptors including KDR and KDRL, which complementarily control intersegmental vessel formation but show distinct binding affinities to VEGF ligands (Bussmann et al., 2008; Covassin et al., 2006; Vogrin et al., 2019). While VEGF-induced signaling pathways in vascular development have been extensively in zebrafish, the potential differences in the signaling pathways of vascular permeability still need further investigation. Although our results support that DDAH1 mediates VEGF-induced vascular permeability in zebrafish, mouse models, and human ECs, it does not exclude the possibility that distinct signaling pathways may be present in VEGF-induced vascular permeability in zebrafish, compared to mammals.

STAR★METHODS

Detailed methods are provided in the online version of this paper and include the following:

- KEY RESOURCES TABLE
- RESOURCE AVAILABILITY
  - Lead contact
  - Materials availability
  - Data and code availability
- EXPERIMENTAL MODEL AND SUBJECT DETAILS
  - Primary cell cultures
  - Zebrafish model
  - Generation of double transgenic, Tg (pKTol2-h70-mC-hVEGF-gcG;Fli:EGFP) fish
  - DDAH1 knockdown in zebrafish
  - Heat-shock induction and imaging of vascular permeability in zebrafish model
  - Mouse model
- METHOD DETAILS
  - Reagents
  - Western blotting
  - Quantification of vascular permeability of zebrafish model
- QUANTIFICATION AND STATISTICAL ANALYSIS

SUPPLEMENTAL INFORMATION

Supplemental information can be found online at https://doi.org/10.1016/j.isci.2021.103189.

ACKNOWLEDGMENTS

We thank Dr. Laura Lewis-Tuffin at Mayo Clinic for assisting with the zebrafish imaging. We thank Drs. Vijay S. Madamsetty, Kequan Chen, Jian Zhu, Santanu Bhattacharya, and Pritam Das in Dr. Mukhopadhyay's laboratory at Mayo Clinic for assisting with the experiments and helpful discussions. We thank Dr. Xun Gong at Massachusetts Institute of Technology for the suggestions on the Matlab-based algorithm. This work was supported by National Institutes of Health [HL140411 and CA78383-20 to D.M., DK117910 to B.J., HL148339 to Y.W.,], Florida Department of Health Cancer Research Chair's Fund Florida [grant number#3J-02 to D.M.], American Heart Association [19CDA34700013 to Y.W.] and Mayo Clinic Center for Clinical and Translational Science (CCaTS) [Ted and Loretta Rogers Cardiovascular Career Development Award Honoring Hugh C. Smith to Y.W.], Department of Defense [W81XWH-20-1-0317 to B.J.], and a Grant-in-Aid of Research, Artistry and Scholarship Program Award #380634 from the Office of Vice President of Research at the University of Minnesota, the Elsa U. Pardee Foundation, and The Hormel

Foundation to L.H.H. The content is solely the responsibility of the authors and does not necessarily represent the official views of the National Institutes of Health.

AUTHOR CONTRIBUTIONS

Conceptualization, D.M., Y.W., L.H.H., R.SA, T.A.K.; Methodology, Y.W., R.SA, L.H.H., K.P.; Validation: Y.W., R.SA, T.A.K., L.H.H., E.W., S.D., K.P.; Resources: Y.C., R.N.R., N.J., B. Ji.; Software: T.A.K., A.T. and R.A.V.; Writing-Original Draft: Y.W.; Writing-Review & Editing: R.SA, T.A.K., L.H.H., R.N.R, Y.C and D.M.; Funding Acquisition: D.M., Y.W., B.J., L.H.H.; Supervision: D.M.

DECLARATION OF INTERESTS

The authors declare no competing interests.

Received: October 30, 2020
Revised: July 12, 2021
Accepted: September 27, 2021
Published: October 22, 2021

REFERENCES

Achan, V., Ho, H.K., Heeschen, C., Stuehlinger, M., Jang, J.J., Kimoto, M., Vallance, P., and Cooke, J.P. (2005). ADMA regulates angiogenesis: genetic and metabolic evidence. Vasc. Med. *10*, 7–14.

Bates, D.O. (2010). Vascular endothelial growth factors and vascular permeability. Cardiovasc. Res. *87*, 262–271.

Bates, D.O., Heald, R.I., Curry, F.E., and Williams, B. (2001). Vascular endothelial growth factor increases Rana vascular permeability and compliance by different signalling pathways. J. Physiol. *533*, 263–272.

Buijs, N., Oosterink, J.E., Jessup, M., Schierbeek, H., Stolz, D.B., Houdijk, A.P., Geller, D.A., and van Leeuwen, P.A. (2017). A new key player in VEGF-dependent angiogenesis in human hepatocellular carcinoma: dimethylarginine dimethylaminohydrolase 1. Angiogenesis *20*, 557–565.

Bussmann, J., Lawson, N., Zon, L., Schulte-Merker, S., and Zebrafish Nomenclature, C. (2008). Zebrafish VEGF receptors: a guideline to nomenclature. Plos Genet. *4*, e1000064.

Carmeliet, P., Ferreira, V., Breier, G., Pollefeyt, S., Kieckens, L., Gertsenstein, M., Fahrig, M., Vandenhoeck, A., Harpal, K., Eberhardt, C., et al. (1996). Abnormal blood vessel development and lethality in embryos lacking a single VEGF allele. Nature *380*, 435–439.

Chavez, M.N., Aedo, G., Fierro, F.A., Allende, M.L., and Egana, J.T. (2016). Zebrafish as an emerging model organism to study angiogenesis in development and regeneration. Front Physiol. *7*, 56.

Chen, H., Tong, X., Lang, L., Jacobson, O., Yung, B.C., Yang, X., Bai, R., Kiesewetter, D.O., Ma, Y., Wu, H., et al. (2017). Quantification of tumor vascular permeability and blood volume by positron emission tomography. Theranostics *7*, 2363–2376.

Claesson-Welsh, L. (2015). Vascular permeability–the essentials. Ups J. Med. Sci. *120*, 135–143.

Claesson-Welsh, L., Dejana, E., and McDonald, D.M. (2021). Permeability of the endothelial barrier: identifying and reconciling controversies. Trends Mol. Med. *27*, 314–331.

Cooke, J.P., and Ghebremariam, Y.T. (2011). DDAH says NO to ADMA. Arterioscler Thromb.Vasc. Biol. *31*, 1462–1464.

Cooksey, C.J. (2014). Quirks of dye nomenclature. 1. Evans blue. Biotech.Histochem. *89*, 111–113.

Covassin, L.D., Villefranc, J.A., Kacergis, M.C., Weinstein, B.M., and Lawson, N.D. (2006). Distinct genetic interactions between multiple Vegf receptors are required for development of different blood vessel types in zebrafish. Proc. Natl. Acad. Sci. U S A *103*, 6554–6559.

Criscuoli, M.L., Nguyen, M., and Eliceiri, B.P. (2005). Tumor metastasis but not tumor growth is dependent on Src-mediated vascular permeability. Blood *105*, 1508–1514.

Cudmore, M.J., Hewett, P.W., Ahmad, S., Wang, K.Q., Cai, M., Al-Ani, B., Fujisawa, T., Ma, B., Sissaoui, S., Ramma, W., et al. (2012). The role of heterodimerization between VEGFR-1 and VEGFR-2 in the regulation of endothelial cell homeostasis. Nat. Commun. *3*, 972.

Curry, F.R., and Adamson, R.H. (2010). Vascular permeability modulation at the cell, microvessel, or whole organ level: towards closing gaps in our knowledge. Cardiovasc. Res. *87*, 218–229.

Dayoub, H., Achan, V., Adimoolam, S., Jacobi, J., Stuehlinger, M.C., Wang, B.Y., Tsao, P.S., Kimoto, M., Vallance, P., Patterson, A.J., and Cooke, J.P. (2003). Dimethylarginine dimethylaminohydrolase regulates nitric oxide synthesis: genetic and physiological evidence. Circulation *108*, 3042–3047.

Di Lorenzo, A., Lin, M.I., Murata, T., Landskroner-Eiger, S., Schleicher, M., Kothiya, M., Iwakiri, Y., Yu, J., Huang, P.L., and Sessa, W.C. (2013). eNOS-derived nitric oxide regulates endothelial barrier function through VE-cadherin and Rho GTPases. J.Cell Sci. *126*, 5541–5552.

Domigan, C.K., Ziyad, S., and Iruela-Arispe, M.L. (2015). Canonical and noncanonical vascular endothelial growth factor pathways: new developments in biology and signal transduction. Arterioscler Thromb.Vasc. Biol. *35*, 30–39.

Dowsett, L., Piper, S., Slaviero, A., Dufton, N., Wang, Z., Boruc, O., Delahaye, M., Colman, L., Kalk, E., Tomlinson, J., et al. (2015). Endothelial dimethylarginine dimethylaminohydrolase 1 is an important regulator of angiogenesis but does not regulate vascular reactivity or hemodynamic homeostasis. Circulation *131*, 2217–2225.

Duval, M., Le Boeuf, F., Huot, J., and Gratton, J.P. (2007). Src-mediated phosphorylation of Hsp90 in response to vascular endothelial growth factor (VEGF) is required for VEGF receptor-2 signaling to endothelial NO synthase. Mol. Biol.Cell *18*, 4659–4668.

Dvorak, H.F. (2021). Reconciling VEGF with VPF: the importance of increased vascular permeability for stroma formation in tumors, healing wounds, and chronic inflammation. Front Cell Dev. Biol. *9*, 660609.

Evans, H.M., and Schulemann, W. (1914). The action of vital stains belonging to the Benzidine group. Science *39*, 443–454.

Ferrara, N. (2005). VEGF as a therapeutic target in cancer. Oncology *69*, 11–16.

Freedman, F.B., and Johnson, J.A. (1969). Equilibrium and kinetic properties of the Evans blue-albumin system. Am. J. Physiol. *216*, 675–681.

Fukumura, D., Gohongi, T., Kadambi, A., Izumi, Y., Ang, J., Yun, C.O., Buerk, D.G., Huang, P.L., and Jain, R.K. (2001). Predominant role of endothelial nitric oxide synthase in vascular endothelial growth factor-induced angiogenesis and vascular permeability. Proc. Natl. Acad. Sci. U S A *98*, 2604–2609.

Gampel, A., Moss, L., Jones, M.C., Brunton, V., Norman, J.C., and Mellor, H. (2006). VEGF regulates the mobilization of VEGFR2/KDR from an intracellular endothelial storage compartment. Blood *108*, 2624–2631.

Gratton, J.P., Lin, M.I., Yu, J., Weiss, E.D., Jiang, Z.L., Fairchild, T.A., Iwakiri, Y., Groszmann, R., Claffey, K.P., Cheng, Y.C., and Sessa, W.C. (2003). Selective inhibition of tumor microvascular permeability by cavtratin blocks tumor progression in mice. Cancer Cell *4*, 31–39.

Heneweer, C., Holland, J.P., Divilov, V., Carlin, S., and Lewis, J.S. (2011). Magnitude of enhanced permeability and retention effect in tumors with different phenotypes: 89Zr-albumin as a model system. J. Nucl. Med. *52*, 625–633.

Hoeppner, L.H., Phoenix, K.N., Clark, K.J., Bhattacharya, R., Gong, X., Sciuto, T.E., Vohra, P., Suresh, S., Bhattacharya, S., Dvorak, A.M., et al. (2012). Revealing the role of phospholipase Cbeta3 in the regulation of VEGF-induced vascular permeability. Blood *120*, 2167–2173.

Hoeppner, L.H., Sinha, S., Wang, Y., Bhattacharya, R., Dutta, S., Gong, X., Bedell, V.M., Suresh, S., Chun, C., Ramchandran, R., et al. (2015). RhoC maintains vascular homeostasis by regulating VEGF-induced signaling in endothelial cells. J.Cell Sci. *128*, 3556–3568.

Hu, X., Atzler, D., Xu, X., Zhang, P., Guo, H., Lu, Z., Fassett, J., Schwedhelm, E., Boger, R.H., Bache, R.J., and Chen, Y. (2011). Dimethylarginine dimethylaminohydrolase-1 is the critical enzyme for degrading the cardiovascular risk factor asymmetrical dimethylarginine. Arterioscler Thromb.Vasc. Biol. *31*, 1540–1546.

Huang, K., Andersson, C., Roomans, G.M., Ito, N., and Claesson-Welsh, L. (2001). Signaling properties of VEGF receptor-1 and -2 homo- and heterodimers. Int. J. Biochem.Cell Biol. *33*, 315–324.

Hulin, J.A., Gubareva, E.A., Jarzebska, N., Rodionov, R.N., Mangoni, A.A., and Tommasi, S. (2019a). Inhibition of dimethylarginine dimethylaminohydrolase (DDAH) enzymes as an emerging therapeutic strategy to target angiogenesis and vasculogenic mimicry in cancer. Front Oncol. *9*, 1455.

Hulin, J.A., Tommasi, S., Elliot, D., and Mangoni, A.A. (2019b). Small molecule inhibition of DDAH1 significantly attenuates triple negative breast cancer cell vasculogenic mimicry in vitro. Biomed.Pharmacother. *111*, 602–612.

Kostourou, V., Robinson, S.P., Cartwright, J.E., and Whitley, G.S. (2002). Dimethylarginine dimethylaminohydrolase I enhances tumour growth and angiogenesis. Br. J. Cancer *87*, 673–680.

Kostourou, V., Robinson, S.P., Whitley, G.S., and Griffiths, J.R. (2003). Effects of overexpression of dimethylarginine dimethylaminohydrolase on tumor angiogenesis assessed by susceptibility magnetic resonance imaging. Cancer Res. *63*, 4960–4966.

Lagendijk, A.K., Gomez, G.A., Baek, S., Hesselson, D., Hughes, W.E., Paterson, S., Conway, D.E., Belting, H.G., Affolter, M., Smith, K.A., et al. (2017). Live imaging molecular changes in junctional tension upon VE-cadherin in zebrafish. Nat. Commun. *8*, 1402.

Lawson, N.D., and Weinstein, B.M. (2002). In vivo imaging of embryonic vascular development using transgenic zebrafish. Dev. Biol. *248*, 307–318.

Li, X., Padhan, N., Sjostrom, E.O., Roche, F.P., Testini, C., Honkura, N., Sainz-Jaspeado, M., Gordon, E., Bentley, K., Philippides, A., et al. (2016). VEGFR2 pY949 signalling regulates adherens junction integrity and metastatic spread. Nat. Commun. *7*, 11017.

Liang, W., Kujawski, M., Wu, J., Lu, J., Herrmann, A., Loera, S., Yen, Y., Lee, F., Yu, H., Wen, W., and Jove, R. (2010). Antitumor activity of targeting SRC kinases in endothelial and myeloid cell compartments of the tumor microenvironment. Clin. Cancer Res. *16*, 924–935.

Lin, M.I., Yu, J., Murata, T., and Sessa, W.C. (2007). Caveolin-1-deficient mice have increased tumor microvascular permeability, angiogenesis, and growth. Cancer Res. *67*, 2849–2856.

Lin, R.L., and Schwartz, R.A. (2006). Hemangiomas of infancy–a clinical review. Acta Dermatovenerol Croat. *14*, 109–116.

Mayhan, W.G. (1994). Nitric oxide accounts for histamine-induced increases in macromolecular extravasation. Am. J. Physiol. *266*, H2369–H2373.

McDonald, D.M. (2001). Angiogenesis and remodeling of airway vasculature in chronic inflammation. Am. J. Respir.Crit. Care Med. *164*, S39–S45.

Murakami, M., Zheng, Y., Hirashima, M., Suda, T., Morita, Y., Ooehara, J., Ema, H., Fong, G.H., and Shibuya, M. (2008). VEGFR1 tyrosine kinase signaling promotes lymphangiogenesis as well as angiogenesis indirectly via macrophage recruitment. Arterioscler Thromb.Vasc. Biol. *28*, 658–664.

Nagy, J.A., Benjamin, L., Zeng, H., Dvorak, A.M., and Dvorak, H.F. (2008). Vascular permeability, vascular hyperpermeability and angiogenesis. Angiogenesis *11*, 109–119.

Pink, D.B., Schulte, W., Parseghian, M.H., Zijlstra, A., and Lewis, J.D. (2012). Real-time visualization and quantitation of vascular permeability in vivo: implications for drug delivery. PLoS ONE *7*, e33760.

Price, C.J., and Raymond, L.A. (1996). Evans blue antagonizes both alpha-amino-3-hydroxy-5-methyl-4-isoxazolepropionate and kainate receptors and modulates receptor desensitization. Mol. Pharmacol. *50*, 1665–1671.

Qin, L., Zhao, D., Xu, J., Ren, X., Terwilliger, E.F., Parangi, S., Lawler, J., Dvorak, H.F., and Zeng, H. (2013). The vascular permeabilizing factors histamine and serotonin induce angiogenesis through TR3/Nur77 and subsequently truncate it through thrombospondin-1. Blood *121*, 2154–2164.

Ramirez, M.M., Kim, D.D., and Duran, W.N. (1996). Protein kinase C modulates microvascular permeability through nitric oxide synthase. Am. J. Physiol. *271*, H1702–H1705.

Ramirez, M.M., Quardt, S.M., Kim, D., Oshiro, H., Minnicozzi, M., and Duran, W.N. (1995). Platelet activating factor modulates microvascular permeability through nitric oxide synthesis. Microvasc. Res. *50*, 223–234.

Rygh, C.B., Qin, S., Seo, J.W., Mahakian, L.M., Zhang, H., Adamson, R., Chen, J.Q., Borowsky, A.D., Cardiff, R.D., Reed, R.K., et al. (2011). Longitudinal investigation of permeability and distribution of macromolecules in mouse malignant transformation using PET. Clin. Cancer Res. *17*, 550–559.

Sasaki, M., North, P.E., Elsey, J., Bubley, J., Rao, S., Jung, Y., Wu, S., Zou, M.H., Pollack, B.P., Kumar, J., et al. (2019). Propranolol exhibits activity against hemangiomas independent of beta blockade. NPJ Precis Oncol. *3*, 27.

Schurmann, B., Wu, X., Dietzel, I.D., and Lessmann, V. (1997). Differential modulation of AMPA receptor mediated currents by evans blue in postnatal rat hippocampal neurones. Br. J. Pharmacol. *121*, 237–247.

Seamens, A., Nieman, E., Losavio, K., Bradley, B., Nelson, K., Chen, K.H., Chen, S., Arbiser, J., and Lawley, L.P. (2018). Salivary levels of angiopoietin-2 in infants with infantile haemangiomas treated with and without systemic propranolol. Exp. Dermatol. *27*, 636–640.

Senger, D.R., Galli, S.J., Dvorak, A.M., Perruzzi, C.A., Harvey, V.S., and Dvorak, H.F. (1983). Tumor cells secrete a vascular permeability factor that promotes accumulation of ascites fluid. Science *219*, 983–985.

Shibuya, M. (2011). Vascular endothelial growth factor (VEGF) and its receptor (VEGFR) Signaling in angiogenesis: a crucial target for anti- and pro-angiogenic therapies. Genes Cancer *2*, 1097–1105.

Sun, Z., Li, X., Massena, S., Kutschera, S., Padhan, N., Gualandi, L., Sundvold-Gjerstad, V., Gustafsson, K., Choy, W.W., Zang, G., et al. (2012). VEGFR2 induces c-Src signaling and vascular permeability in vivo via the adaptor protein TSAd. J. Exp. Med. *209*, 1363–1377.

Teuwen, L.A., Geldhof, V., Pasut, A., and Carmeliet, P. (2020). Author Correction: COVID-19: the vasculature unleashed. Nat. Rev. Immunol. *20*, 448.

Ung, C.Y., Lam, S.H., Hlaing, M.M., Winata, C.L., Korzh, S., Mathavan, S., and Gong, Z. (2010). Mercury-induced hepatotoxicity in zebrafish: in vivo mechanistic insights from transcriptome analysis, phenotype anchoring and targeted gene expression validation. BMC Genom. *11*, 212.

Vogrin, A.J., Bower, N.I., Gunzburg, M.J., Roufail, S., Okuda, K.S., Paterson, S., Headey, S.J., Stacker, S.A., Hogan, B.M., and Achen, M.G. (2019). Evolutionary differences in the Vegf/Vegfrcode reveal organotypic roles for the endothelial cell receptor Kdr in developmental lymphangiogenesis. Cell Rep. *28*, 2023–2036.e2024.

Wang, L., Astone, M., Alam, S.K., Zhu, Z., Pei, W., Frank, D.A., Burgess, S.M., and Hoeppner, L.H. (2021). Suppressing STAT3 activity protects the endothelial barrier from VEGF-mediated vascular permeability. Dis Model Mech. https://doi.org/10.1242/dmm.049029.

Wang, L., Zeng, H., Wang, P., Soker, S., and Mukhopadhyay, D. (2003). Neuropilin-1-mediated vascular permeability factor/vascular endothelial growth factor-dependent endothelial cell migration. J. Biol. Chem. *278*, 48848–48860.

Weis, S., Cui, J., Barnes, L., and Cheresh, D. (2004). Endothelial barrier disruption by VEGF-mediated Src activity potentiates tumor cell extravasation and metastasis. J.Cell Biol. *167*, 223–229.

Wu, H.M., Huang, Q., Yuan, Y., and Granger, H.J. (1996). VEGF induces NO-dependent hyperpermeability in coronary venules. Am. J. Physiol. *271*, H2735–H2739.

Yamamura, H., Ugawa, S., Ueda, T., and Shimada, S. (2005). Evans blue is a specific antagonist of the human epithelial Na+ channel delta-subunit. J. Pharmacol. Exp. Ther. *315*, 965–969.

Yang, K.S., Lim, J.H., Kim, T.W., Kim, M.Y., Kim, Y., Chung, S., Shin, S.J., Choi, B.S., Kim, H.W., Kim, Y.S., et al. (2014). Vascular endothelial growth factor-receptor 1 inhibition aggravates diabetic nephropathy through eNOS signaling pathway in db/db mice. PLoS ONE *9*, e94540.

Yao, L., Xue, X., Yu, P., Ni, Y., and Chen, F. (2018). Evans blue dye: a revisit of its applications in biomedicine. Contrast Media Mol. Imaging *2018*, 7628037.

Yuan, Q., Bai, Y.P., Shi, R.Z., Liu, S.Y., Chen, X.M., Chen, L., Li, Y.J., and Hu, C.P. (2014). Regulation of endothelial progenitor cell differentiation and function by dimethylarginine dimethylaminohydrolase 2 in an asymmetric dimethylarginine-independent manner. Cell Biol. Int. *38*, 1013–1022.

Yuan, Y., Granger, H.J., Zawieja, D.C., and Chilian, W.M. (1992). Flow modulates coronary venular permeability by a nitric oxide-related mechanism. Am. J. Physiol. *263*, H641–H646.

Zhang, P., Hu, X., Xu, X., Chen, Y., and Bache, R.J. (2011). Dimethylarginine dimethylaminohydrolase 1 modulates endothelial cell growth through nitric oxide and Akt. Arterioscler Thromb.Vasc. Biol. *31*, 890–897.

Zhang, P., Xu, X., Hu, X., Wang, H., Fassett, J., Huo, Y., Chen, Y., and Bache, R.J. (2013). DDAH1 deficiency attenuates endothelial cell cycle progression and angiogenesis. PLoS ONE *8*, e79444.

Zhang, X., and Simons, M. (2014). Receptor tyrosine kinases endocytosis in endothelium: biology and signaling. Arterioscler Thromb.Vasc. Biol. *34*, 1831–1837.

Zhang, Z., Neiva, K.G., Lingen, M.W., Ellis, L.M., and Nor, J.E. (2010). VEGF-dependent tumor angiogenesis requires inverse and reciprocal regulation of VEGFR1 and VEGFR2. Cell Death Differ. *17*, 499–512.

STAR★METHODS

KEY RESOURCES TABLE

REAGENT or RESOURCE	SOURCE	IDENTIFIER
Antibodies		
β-actin antibody	Sigma-Aldrich	#A2228; RRID:AB_476697
VEGFR2 antibody	Cell Signaling Technology	#2479; RRID:AB_2212507
phosphorylated VEGFR2 Tyrosine 951 antibody	Cell Signaling Technology	#2471;RRID:AB_331021
phosphorylated VEGFR2 Tyrosine 1175 antibody	Cell Signaling Technology	#2478; RRID:AB_331377
FAK antibody	Cell Signaling Technology	#3285; RRID:AB_2269034
phosphorylated FAK Tyrosine 397 antibody	Cell Signaling Technology	#3283;RRID:AB_2173659
c-Src antibody	Cell Signaling Technology	#2109; RRID:AB_2106059
phosphorylated c-Src Tyrosine 416 antibody	Cell Signaling Technology	#2101;RRID:AB_331697
DDAH2 antibody	Proteintech	#14966-1-AP; RRID:AB_2276973
DDAH1 antibody	Abcam	#ab180599
Chemicals, peptides, and recombinant proteins		
Recombinant human VEGF	R&D	#293-VE-010
L-NAME	Cayman Chemical	#80210
DAF-FM Diacetate (4-Amino-5-Methylamino-2′,7′-DifluorofluoresceinDiacetate)	ThermoFisher Scientific	#D23844
Critical commercial assays		
Nitric Oxide Assay Kit (Fluorometric)	Abcam	#ab65327
Experimental models: Cell lines		
HUVECs	Lonza	#CC-2517
Human retinal microvascular endothelial cells	Cell System	#ACBRI 181
Experimental models: organisms/strains		
DDAH1 transgenic mouse	Jackson Laboratory	RRID:IMSR_JAX:005863
DDAH1 knockout mouse	Hu et al., 2011	N/A
Tg (*pKTol2- h70-mC-hVEGF-gcG;Fli:EGFP*) fish	This paper	N/A
Tg (*pKTol2-h70-mC-hVEGF-gcG*) fish	Hoeppner et al., 2012	N/A
Tg (*Fli:EGFP*) fish	Lawson and Weinstein, 2002	ZFIN: ZDB-TGCONSTRCT-070117-94
Oligonucleotides		
DDAH1 MO	Gene Tools	5′-CTGTCTGCTGAGGTGTGTTTGTACC-3′
Nonspecific MO	Gene Tools	5′-CATCATATTCAGGGTAGTCGAAGTT-3′
Recombinant DNA		
DDAH1 cDNA ORF Clone	Sino Biological	#HG18343-U
pGIPZ-DDAH1 shRNA	Horizon Discovery	Targeting sequence: 5′-ACACATTAGAAAGATCTGC-3′
pGIPZ-DDAH1 shRNA (SMARTvector, with no fluorescent reporter)	Horizon Discovery	Targeting sequence: 5′-TTCAGTGCCGCATTGTTCT-3′
pkTol2-h70-mC-hVEGF-gcG plasmid	Hoeppner et al., 2012	N/A
pGag.Pol packing plasmid	Wang et al., 2003	N/A
pVSV-G packing plasmid	Wang et al., 2003	N/A

(*Continued on next page*)

Continued

REAGENT or RESOURCE	SOURCE	IDENTIFIER
Software and algorithms		
Permeability quantification algorithm in zebrafish model	This paper	https://data.mendeley.com/datasets/6wp3jnwd3y/2
GraphPad Prism 5	GraphPad Software	RRID:SCR_002798
ImageLab software	Bio-Rad	RRID:SCR_014210
BioRender	BioRender	RRID:SCR_018361

RESOURCE AVAILABILITY

Lead contact

Further information and requests for resources and reagents should be directed to and will be fulfilled by the lead contact Dr. Debabrata Mukhopadhyay (mukhopadhyay.debabrata@mayo.edu).

Materials availability

This study did not generate new unique reagents.

Data and code availability

The Matlab-based algorithm has been deposited at the repository of Mendeley Data. Accession number is listed in the key resources table.

EXPERIMENTAL MODEL AND SUBJECT DETAILS

Primary cell cultures

HUVEC (Lonza) from a single female donor were passaged in EBM endothelial cell basal media supplemented with EGM-MV SingleQuots (Lonza). Human retinal microvascular endothelial cells (Cell System) from a male donor were cultured in Complete Classic Medium with serum and CultureBoost™ (Cell System), which were authenticated by >95% positive fluorescent staining of cytoplasmic VWF and CD31, and cytoplasmic uptake of Di-I-Ac-LDL, and <1% immunofluorescent staining of glial fibrillary acidic protein, glutamine synthetase, glial antigen 2 and platelet derived growth factor receptor-β, by the manufacturer.

Zebrafish model

Zebrafish were used and maintained according to Institutional Animal Care and Use Committee (IACUC) guidelines at Mayo Clinic, Jacksonville. Zebrafish embryos were used in experiments, so no zebrafish gender information was provided in this study.

Generation of double transgenic, Tg (pKTol2-h70-mC-hVEGF-gcG;Fli:EGFP) fish

To better visualize the blood vasculature and the vascular permeability in zebrafish embryos, we have generated a double transgenic system in zebrafish by crossing the heat shock-inducible *Tg* (*pKTol2-h70-mC-hVEGF-gcG*) fish (Hoeppner et al., 2012) with the *Tg* (*Fli:EGFP*) fish, which express enhanced green fluorescent protein (EGFP) in all blood vessels throughout embryogenesis (Lawson and Weinstein, 2002). To generate the heat-inducible *Tg* (*pKTol2-h70-mC-hVEGF-gcG*) fish, 1-cell stage SWT zebrafish embryos were coinjected with 2 nL of pkTol2-h70-mC-hVEGF-gcG plasmid (12.5 ng/μL) and transposase mRNA (12.5 ng/μL) and then potential founders were screened by expression of enhanced green fluorescent protein (EGFP) in their eyes, which was driven by the lens-specific γ-crystallin promoter. Then these founders were raised to adulthood and cross with *Tg* (*Fli:EGFP*) fish and F1 progenies obtained from their crosses were used to identify true transgenics. The lines with low background but high heat-shock induction of mCherry (Figure 1A) were selected and Cre mRNA was injected as described before (Hoeppner et al., 2012).

DDAH1 knockdown in zebrafish

A translation blocking DDAH1 MO (5′-CTGTCTGCTGAGGTGTGTTTGTACC-3′) was designed and purchased from Gene Tools. On the day of microinjection, the one-cell embryos were arranged on a agarose

plate as described earlier (Hoeppner et al., 2012) and microinjected with DDAH1 MO (100 μM, 4.5 nL) and nonspecific MO (5′-CATCATATTCAGGGTAGTCGAAGTT-3′ (100 μM, 4.5 nL) as a control, respectively, using PL1-90 microinjector (Harvard Apparatus, Holliston, MA).

Heat-shock induction and imaging of vascular permeability in zebrafish model

The experiments were performed as previously described with minor modifications (Hoeppner et al., 2012). Capped Cre mRNA was synthesized using mMessge mMachine T3 transcription kit (Thermo Fisher Scientific) and microinjected into embryos at 1–2 cell stage (1.5 nl, 12.5ng/ul). At 3-days post-fertilization (3-dpf), embryos were anaesthetized in 0.015% tricaine methanesulfonate (Western Chemical, Inc) and microangiography was performed by inserting a glass microneedle (World precision Instruments, Sarasota, FL) through the pericardium directly into ventricle as described previously (Hoeppner et al., 2012). Texas Red-dextran with a molecular weight of 70 kDa solubilized in embryo medium at a 2 mg/mL concentration and a total of 4.5 nL was injected. Basal vascular permeability in zebrafish was defined as no exposure to heat shock. Acute vascular permeability was induced by 1 heat-shock induction, which was performed by transferring the zebrafish from 28.5°C to 37°C embryo water and incubating at 37°C for 30 minutes. Chronic vascular permeability was defined as three 30-minute heat-shock inductions of VEGF separated by 30 minutes at 28.5°C. Images were acquired immediately after heat-shock using a Zeiss LSM 880 confocal microscope using standard FITC and dsRed filter sets and 10X objective at room temperature.

Mouse model

Animal care and experimental procedures were performed under protocols approved by the IACUC of Mayo Clinic. DDAH1 transgenic mice (RRID:IMSR_JAX:005863) with global expression of human DDAH1 under control of β-actin promoter were obtained from Jackson Laboratory (Dayoub et al., 2003). DDAH1 knockout mice were bred, genotyped and housed as previously described (Hu et al., 2011). Age-matched male wild type (WT) mice (C57BL/6J) were used as control. The mice were housed in a conventional facility at Mayo Clinic, Jacksonville, with a reverse 12-h light/12-h dark cycle and ad libitum access to food and water. Miles assay was performed as previously described (Li et al., 2016; Qin et al., 2013) with minor modifications. Briefly, flank hair skin was clipped 1 day before the experiment. Mice received intraperitoneal injection of pyrilamine maleate salt (4 mg per kg body weight in 0.9% saline, Sigma) to inhibit unspecific histamine release 30 min before Evans blue (Sigma) tail vein injection (100 μl 1% Evans blue in sterile saline/30 g body weight). Intradermal injection of VEGF (50 ng in 50 μl) or sterile saline was performed 20 min after Evans blue administration. Thirty minutes after the VEGF injection, flank injection sites were imaged and excised. Evans blue was extracted from the flank skins through incubating with formamide at 55°C for 48h, measured using a Spectramax plate reader at 610 nm and expressed as ratios of absorbance at 610 nm to weight of tissue. The investigators who performed the injection and tissue harvest were blinded to the genotypes of mice.

METHOD DETAILS

Reagents

Recombinant VEGF was purchased from R&D. DAF-AM was purchased from Life Technologies and was used according to the manufacture's protocols. Nitrite/nitrate levels in the conditioned medium were analyzed with a Nitric Oxide Assay Kit (Fluorometric) (ab65327) after deproteinization with a 3 kDa Spin column (Millipore Sigma). β-actin antibody (#A2228; RRID:AB_476697) was purchased from Sigma-Aldrich. L-NAME was obtained from Cayman Chemical. Antibodies against total VEGFR2 (#2479; RRID:AB_2212507), phosphorylated VEGFR2 Tyrosine 951 (#2471; RRID:AB_331021), phosphorylated VEGFR2 Tyrosine 1175 (#2478; RRID:AB_331377), FAK (#3285; RRID:AB_2269034), phosphorylated FAK Tyrosine 397 (#3283; RRID:AB_2173659), c-Src (#2109; RRID:AB_2106059) and phosphorylated c-Src Tyrosine 416 (#2101; RRID:AB_331697) were from Cell Signaling Technology. DDAH2 antibody (#14966-1-AP; RRID:AB_2276973) was from Proteintech. DDAH1 antibody (#ab180599) was purchased from Abcam. Short hairpin RNA (shRNA) for human DDAH1 and controls were from Open Biosystems (Huntsville, AL, USA). The DDAH1 shRNA targeting sequence was 5′-ACACATTAGAAAGATCTGC-3′. Lentivirus of DDAH1 shRNA and control shRNA was prepared in 293T cells transfected with targeted gene (pGIPZ-DDAH1 shRNA and pGIPZ-control shRNA from Dharmacon), pGag.Pol, and pVSV-G encoding the cDNAs of the proteins that are required for virus packing as previously described (Wang et al., 2003). After infection, 2 μg/ml of puromycin was added to the medium for antibiotic selection. An independent lentivirus DDAH1 shRNA SMARTvector with no fluorescent reporter (5′-TTCAGTGCCGCATTGTTCT-3′) was used in the DAF-FAM

assay of nitric oxide. DDAH1 cDNA ORF Clone in Cloning Vector was purchased from Sino Biological (PA, USA) and used to construct retrovirus expressing DDAH1 as previously described (Wang et al., 2003). Graphic summery was created using BioRender (RRID:SCR_018361).

Western blotting

Total cellular protein and zebrafish embryo protein were extracted by RIPA lysis buffer supplemented with proteinase inhibitor cocktail and phosphate inhibitor (Thermo Fisher Scientific). The cellular proteins were subjected to sodium dodecyl sulfate-polyacrylamide gel electrophoresis and immunoblotted with primary antibodies followed by secondary antibodies conjugated with horseradish peroxidase (Santa Cruz). The signals were detected with SuperSignal™ West Femto Maximum Sensitivity Substrate (Thermo Fisher Scientific) using a Bio-Rad ChemiDoc Imaging Systems. Bands intensities were analyzed with ImageLab software (RRID:SCR_014210). Full blots are now included in the supplementary figures (Figures S1, S4, S6, and S9). A single loading control was used for all those western blots, because one blot was cut and probed with antibodies against the phosphorylated VEGFR2 (~210–230 kDa), FAK (~120 kDa) and c-Src (~60 kDa), and DDAH1 (~37 kDa). Then these blots were processed with stripping buffer and probed with antibodies of total VEGFR2, FAK and Src, β-Actin (~42 kDa) and DDAH2 (~25 kDa). A secondary gel was loaded at the same time to examine a different phosphorylated site of VEGFR2 and then followed by detection of total VEGFR2.

Quantification of vascular permeability of zebrafish model

Raw ".czi" images were acquired by employing confocal microscopy. Each individual image comprising of multiple z-stacks, which were preprocessed using the Zeiss inbuilt image processing software to generate a maximum intensity projection image. Matlab programming platform was used to process the maximum intensity projection images of normal as well as various heat shock treatments. Image processing toolbox comprising of various inbuilt functions was employed to design an algorithm that enabled quantification of dye leakage upon various treatments. Briefly, a flowchart corresponding to the algorithm is described below:

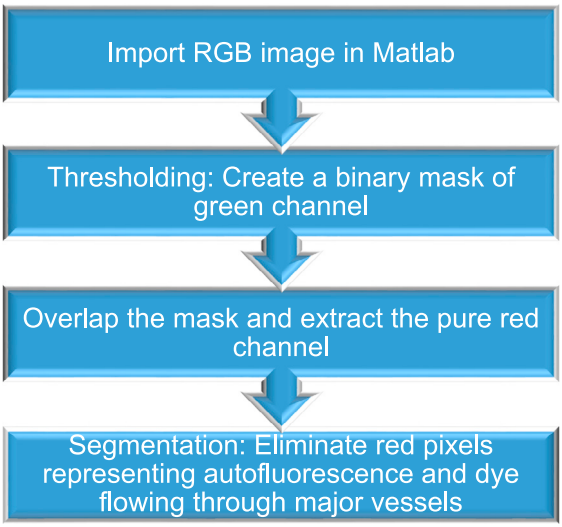

The algorithm involves the use of thresholding and segmentation techniques. Specifically, thresholding technique was used to implement a binary mask. A binary mask comprised of a grayscale image corresponding to only the green pixels which was overlapped with the original image to eliminate all the features corresponding to green pixels such as major intersegmental vessel (ISV). Post masking, the red pixels were

subjected to a segmentation technique to remove any small vessels or capillaries that do not indicate leakage.

QUANTIFICATION AND STATISTICAL ANALYSIS

All analyses were performed using GraphPad Prism 5 (GraphPad Software, RRID:SCR_002798). All the values are expressed as means ± SD. Statistical significance was determined using 2-sided Student t test and a value of $p < .05$ was considered significant.